Molecular Therapy
Nucleic Acids
Original Article

A transferable SARS-CoV-2 IRES module enables dual translation initiation for enhanced antigen expression in COVID-19 mRNA vaccines

Han Young Seo,[1] Haewon Jung,[1] Se-Young Lee,[1] Hae-Gwang Jung,[1,2] Hee Cho,[1] Yu-Min Son,[1] Yeonju Bak,[1] Seo-Yeon Hwang,[1] Jung-Hee Kim,[2] In Ho Park,[3,5] Jeon-Soo Shin,[3,4,5] and Jong-Won Oh[1,2]

[1]Department of Biotechnology, Yonsei University, 50 Yonsei-ro, Seodaemun-gu, Seoul 03722, Republic of Korea; [2]RpexBio Inc., 117-3, Hoegi-ro, Dongdaemun-gu, Seoul Biohub Global Center, Seoul 02455, Republic of Korea; [3]Department of Biomedical Sciences, Yonsei University College of Medicine, Seoul 03722, Republic of Korea; [4]Department of Microbiology, Yonsei University College of Medicine, Seoul 03722, Republic of Korea; [5]Institute of Immunology and Immunological Diseases, Yonsei University College of Medicine, Seoul 03722, Republic of Korea

mRNA vaccines are a versatile platform for infectious disease prevention and therapeutic applications, yet their performance is limited by exclusive reliance on cap-dependent translation, which is markedly suppressed under hypoxia and cellular stress. Here, we report a hybrid 5′ untranslated region (5′UTR) that enables dual translation initiation via both cap-dependent and internal ribosome entry site (IRES) mechanisms. This element integrates a minimal stem-loop 4.5–5 module (SL4.5–5) from the SARS-CoV-2 genomic 5′UTR, in which a conserved 5′-UUUCGU-3′ motif within the SL5 loops is essential for function. Incorporating the SL4.5–5 module downstream of conventional 5′UTRs confers cap-independent translation capacity and enhances overall translation efficiency under translation-restrictive conditions such as hypoxia. When applied to the 5′UTRs of clinically validated COVID-19 vaccines, this module improves antigen expression in both modified and unmodified mRNAs. Notably, unmodified Omicron BA.5 and XBB.1.5 mRNA vaccines containing this element elicited potent humoral and cellular immune responses at sub-microgram doses, comparable to those induced by the approved N1-methylpseudouridine-incorporated mRNA vaccine, raxtozinameran. These findings identify SL4.5–5 as a modular IRES element that enables dual translation initiation, promoting efficient protein synthesis under cap-dependent translation-restrictive conditions and expanding the functional landscape of mRNA vaccines and therapeutics beyond cap-dependent limitations.

INTRODUCTION

The remarkable success of mRNA vaccines during the COVID-19 pandemic established this technology as a leading platform for rapid vaccine development against emerging infectious diseases, including those caused by rapidly evolving viruses.[1] The basic design of mRNA vaccines and therapeutics consists of an open reading frame (ORF) encoding the target protein, flanked by untranslated regions (UTRs) and a poly(A) tail. Among these, the 5′UTR is a critical element that orchestrates protein expression initiation by recruiting translation initiation factors.[1–3] Its design thus directly influences the efficiency and kinetics of antigen expression.[3]

In eukaryotic cells, translation is generally initiated through the cap-dependent pathway.[2] The 5′ cap structure recruits the eukaryotic initiation factor 4F (eIF4F) complex, including the cap-binding protein eIF4E, thereby driving ribosome loading at the 5′UTR.[2] This mechanism represents the canonical mode of translation initiation under normoxic conditions. In contrast, in uncapped RNAs, translation may also proceed through internal ribosome entry site (IRES), which recruits ribosomes independent of the 5′ cap.[4,5] Such IRES-mediated initiation is widely exploited by RNA viruses to ensure protein synthesis under conditions that suppress host cap-dependent translation.[4,5]

Approved COVID-19 mRNA vaccines rely exclusively on cap-dependent translation and employ optimized 5′UTRs to maximize cap-dependent translation and antigen yields.[1,6] For example, Moderna's mRNA-1273 (Spikevax) uses a synthetic 57-nt 5′UTR, while the Pfizer-BioNTech BNT162b2 vaccine employs a sequence derived from the 5′UTR of human α-globin (*HBA1*) mRNA.[6] In contrast, CureVac's first-generation vaccine CVnCoV used a very short artificial 5′UTR sequence.[7] Its second-generation vaccine, CV2CoV, incorporated a longer, optimized 5′UTR derived from human hydroxysteroid 17β-dehydrogenase 4 (*HSD17B4*), resulting in improved antigen expression and enhanced immunogenicity.[7] These examples highlight the 5′UTR as a key determinant of mRNA translational potency and overall vaccine performance.

While optimized under the controlled environment of *in vitro* cell culture, typically maintaining oxygen levels around 21%, 5′UTRs

Received 11 November 2025; accepted 2 March 2026;
https://doi.org/10.1016/j.omtn.2026.102886.

Correspondence: Jong-Won Oh, Department of Biotechnology, Yonsei University, 50 Yonsei-ro, Seodaemun-gu, Seoul 03722, Republic of Korea.
E-mail: jwoh@yonsei.ac.kr

Published by Elsevier Inc. on behalf of The American Society of Gene and Cell Therapy.
This is an open access article under the CC BY-NC-ND license (http://creativecommons.org/licenses/by-nc-nd/4.0/).

that rely entirely on cap-dependent translation can markedly reduce target expression in environments where diverse physiological stresses restrict cap-dependent translation. In fact, *in vivo* translation of mRNA vaccines and therapeutics often takes place under suboptimal oxygen conditions, including intramuscular tissues, draining lymph nodes,[8] tumor microenvironments,[9] and poorly vascularized deep tissues.[10] Moreover, cap-dependent translation is inhibited in senescent or stressed cells through mTOR pathway suppression and dephosphorylation of 4E-binding protein 1 (4E-BP1), as well as by cleavage of eIF4G by viral proteases or caspases activated during apoptosis.[11,12] These dynamic, translation-restrictive environments can markedly limit antigen persistence and dampen immune responses. Therefore, the performance of the mRNA vaccine can be further improved if the mRNA 5′UTR is resilient to these cap-dependent translation-unfavorable conditions.

In this study, we aimed to overcome the limitations of conventional mRNA vaccines by creating an mRNA that can robustly express protein via both cap-dependent and cap-independent mechanisms, ensuring sustained antigen production even under hypoxic or cellular stress conditions. We developed a hybrid 5′UTR that integrates a modular IRES element derived from the SARS-CoV-2 (SCoV2) 5′UTR. This element features a minimal *cis*-acting stem-loop 4.5–5 (SL4.5–5), which confers IRES activity and is notably absent from viral subgenomic RNAs (sgRNAs), underscoring its unique role in the translation of genomic RNA (gRNA). When incorporated into SCoV2 spike-encoding mRNAs, the optimized hybrid 5′UTR sustained translation and antigen expression under eIF4E-restrictive conditions, including hypoxia. Unmodified mRNA COVID-19 vaccines carrying the IRES module elicited robust humoral immunity at low doses and conferred protective immunity in mice, achieving immunological benchmarks comparable to or exceeding those of approved mRNA vaccines. We demonstrate that this approach provides a framework for developing next-generation RNA vaccines and therapeutics with enhanced potency, durability, and translational resilience in challenging environments.

RESULTS

Identification of a minimal *cis*-acting IRES element in the SCoV2 gRNA 5′UTR that sustains translation under hypoxia

SCoV2 infection frequently causes severe lung tissue damage, resulting in hypoxemia,[13] which can inhibit mammalian target of rapamycin (mTOR) signaling.[14] This leads to dephosphorylation of the translational repressor eIF4E-binding protein 1 (4E-BP1), resulting in suppression of cap-dependent translation[14] (Figure 1A). Since both SCoV2 gRNA and its sgRNAs (Figure S1A) are 5′-capped,[15] we hypothesized that the virus may utilize a *cis*-acting RNA element within its 5′UTR to sustain gene expression when cap-dependent translation is compromised.

To investigate this, we generated a recombinant, noninfectious SCoV2 subgenomic replicon (sgRep, G-clade) expressing Nano luciferase (Nluc) via the Spike (S) sgRNA 5′UTR, as well as the nucleocapsid (N) protein under control of its own sgRNA 5′UTR (Figures 1B and 1C, top). sgRep RNA was transfected into HEK293T cells cultured under either normoxic (21% O_2) or hypoxic (1% O_2) conditions. As expected, hypoxic stress induced HIF1α accumulation and dephosphorylation of 4E-BP1 (Figure 1C, left). N protein expression was completely abolished in cells transfected after 6 h of hypoxic pre-exposure (Figure 1C, middle), and N sgRNA copy numbers were reduced by ∼3 $\log_{10}$ compared to normoxia (Figure S1B). By contrast, capped gRNA 5′UTR-directed Nsp1 expression was only modestly affected, with its RNA levels remaining unchanged. Furthermore, Nluc expression directed by the S sgRNA 5′UTR was diminished by 90.3% in hypoxia (Figure 1C, right). These results suggest the presence of a *cis*-acting sequence within the gRNA 5′UTR that supports cap-independent translation during cap-dependent impairment.

The direct assessment of the IRES activity of SCoV2 gRNA 5′UTR was carried out using bicistronic reporter assays. In the assay, we included a 301-nt-long gRNA 5′UTR derivative spanning the first 36 nt of ORF1a, designed to preserve the structural integrity of the SL5 in the intergenic region. Both the gRNA 5′UTR and its extended derivative exhibited comparable IRES activity (Figure 1D).

To validate the IRES function in an mRNA context, we generated uncapped, polyadenylated mRNAs containing either the gRNA 5′UTR derivative (with the authentic ORF1ab AUG disrupted by G268A substitution) or the N sgRNA 5′UTR placed upstream of an ORF encoding the Omicron BA.5 spike antigen [BA.5 S(SA), harboring R685S and R815A substitutions][16] (Figure 1E, left). In mitochondrial antiviral-signaling protein (MAVS) knockout Huh7 cells, which minimize interferon-β induction in response to uncapped RNA, and HEK293T cells, the gRNA derivative directed robust cap-independent translation, whereas the N sgRNA 5′UTR yielded minimal expression (Figure 1E, right). Similar results were obtained using a firefly luciferase reporter (Figure S2A). We designated the 301-nt-long extended 5′UTR sequence with the G268A substitution as the SCoV2 IRES. Its intergenic IRES activity was similar to that of the hepatitis C virus (HCV) IRES (Figure S2B).

Structural mapping revealed that SL4.5 and SL5 were indispensable for the IRES activity, while deletion of SL4 produced an IRES even more active than the full-length sequence, suggesting an inhibitory role due to a short, upstream ORF (uORF) within SL4 (Figures 1F and S2C).

Together, these findings identify a minimal *cis*-acting RNA element within the SCoV2 gRNA 5′UTR that confers IRES function, sustaining translation under hypoxic conditions that inhibit cap-dependent initiation, in contrast to subgenomic RNA 5′UTRs, which lack such activity.

Identification of conserved residues and motifs promoting IRES activity in the evolving SCoV2 5′UTR

Mutation profile analysis of 3,434 representative SCoV2 genomes (from a total of 5,130,239 sequences in GISAID as of November 14, 2021) identified several lineage-specific mutations within the defined IRES region (Figure 2A). Following the initial Wuhan strain,

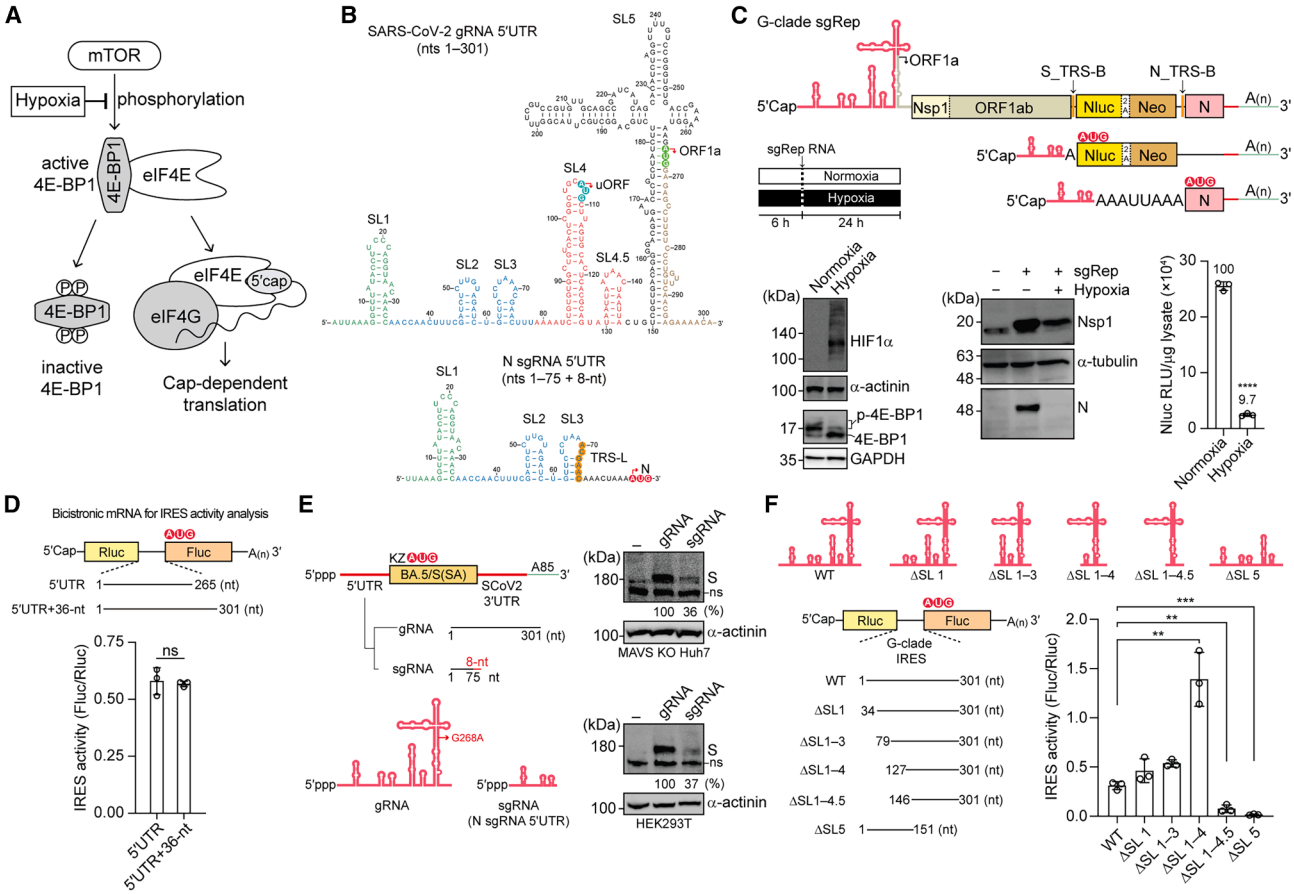

Figure 1. Identification and mapping of a minimal IRES element in the SCoV2 gRNA 5′UTR

(A) Schematic of hypoxia-induced inhibition of cap-dependent translation via mTOR pathway suppression. mTOR, mammalian target of rapamycin; eIF4E, eukaryotic translation initiation factor 4E; 4E-BP1, eIF4E-binding protein 1; eIF4G, eukaryotic translation initiation factor 4G. (B) Predicted secondary structure of the G-clade SCoV2 genomic 5′UTR (including the first 36-nt of ORF1a) and N sgRNA 5′UTR. uORF, short upstream ORF; TRS-L, transcription regulatory sequence leader. (C) Cap-dependent translation efficiency of SCoV2 genomic and subgenomic RNAs in subgenomic replicon (sgRep) assays. Schematic of SCoV2 sgRep RNA products: (1) full-length sgRep (top), 2) nanoluciferase (Nluc)-coding sgRNA (middle) produced via TRS-L and S gene body TRS (S_TRS-B) interaction, and (3) N protein-encoding sgRNA (bottom) produced via TRS-L and N_TRS-B interaction. HEK293T cells transfected with LNP-encapsulated sgRep RNA were cultured under normoxic (21% O_2) or hypoxic (1% O_2) conditions and analyzed by immunoblotting and luciferase assay. (D) IRES activities of indicated viral *cis*-acting RNA elements. Schematic of bicistronic mRNA transcribed from pDual-IRES plasmid harboring G-clade SCoV2 5′UTR and its ORF1a-extended derivative; reporter activities were quantified at 48 h in HEK293T cells. (E) Comparative cap-independent translation of uncapped, Omicron BA.5 spike mRNA harboring SCoV2 gRNA-derived IRES (with a G268A substitution) or the sgRNA 5′UTR. Huh7 MAVS KO or HEK293T cells were transfected with 5′-triphosphate mRNAs (5 μg per well, six-well) and analyzed at 4 h post-transfection. Spike antigen expression levels were quantified by densitometric analysis using ImageJ. (F) Predicted RNA secondary structures of full-length SCoV2 IRES and its deletion mutants assayed in dual reporter format as in (D). In (C, D, and F), data represent mean ± SD of three independent experiments. Statistical significance was determined by an unpaired two-tailed Student's *t* test (**$p < 0.01$; ***$p < 0.001$; ****$p < 0.0001$; ns, not significant).

the G-clade acquired a C_{241}-to-U (C241U) substitution within SL5b, while the Delta variant introduced an additional G_{210}-to-U (G210U) substitution in SL5a (Figure 2B). Of these two mutations, only the U_{241} residue in the SL5b loop persisted in subsequent lineages (Figure S3). Dual-reporter assays showed that the ancestral Wuhan 5′UTR exhibited higher IRES activity than either the G-clade or Delta variants (Figure 2B), suggesting that these substitutions attenuate viral translation efficiency. Notably, the U_{210} residue in the Delta variant had no significant effect on IRES activity compared to the G-clade, indicating this mutation is functionally silent.

A conserved 5′-UUU(C_{241})GU-3′ loop motif in SL5b is mirrored in SL5a, where the C_{203} residue occupies the equivalent position. Functional interrogation demonstrated that mutation of either the C_{241} in SL5b or the C_{203} in SL5a reduced IRES activity, while combined substitutions produced the strongest defect (Figure 2C). These findings establish that the C_{203} and C_{241} nucleotides are critical for IRES function.

In addition to supporting IRES activity, the Wuhan 5′UTR bearing intact C_{203} and C_{241} residues also enhanced cap-dependent

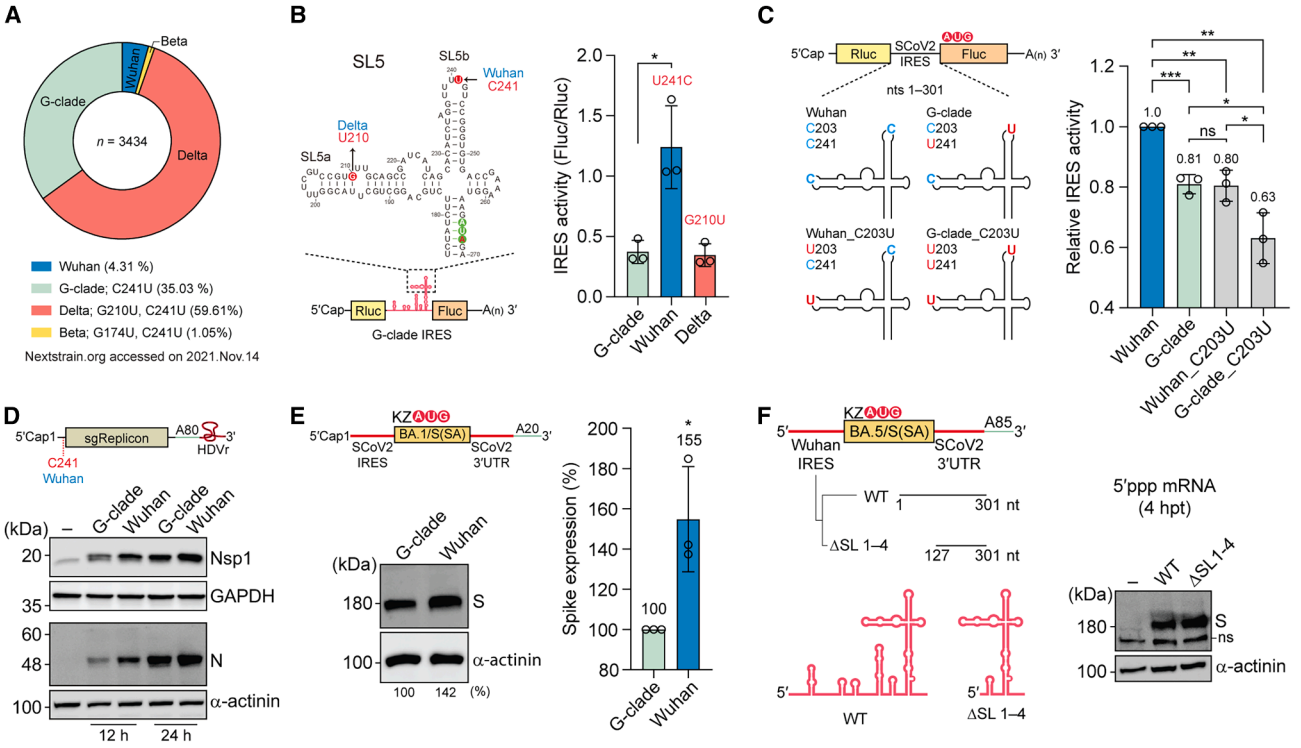

Figure 2. The conserved 5′-UUUCGU-3′ motif in SL5a and SL5b is essential for SARS-CoV-2 IRES activity

(A) Distribution of mutations in the SCoV2 5′UTR across variants, based on Nextstrain.org data (accessed November 14, 2021). The donut chart shows the relative prevalence of variant-specific substitutions. (B and C) The conserved 5′-UUUCGU-3′ sequence in the apical loops of SL5a and SL5b is crucial for IRES function. IRES activity of SCoV2 variants (B) and Wuhan IRES mutants (C) was assessed using the bicistronic reporter assay as in Figure 1D. (D) Immunoblots of viral proteins expressed from gRNA and sgRNA of SCoV2 sgRep carrying 5′UTRs from either G-clade or Wuhan strain. (E) Enhanced expression of Omicron BA.1 spike antigen from capped mRNAs harboring the Wuhan IRES. HEK293T cells were transfected with capped mRNAs (3 μg per well, six-well plates) manually encapsulated in LNPs. Spike antigen expression was analyzed by immunoblot at 24 h post-transfection. Shown is a representative image from three independent biological replicates. (F) SL4.5–5 constitutes the minimal IRES element supporting cap-independent translation. Schematic of uncapped mRNAs used to evaluate IRES activity. Spike antigen expression level was analyzed as in Figure 1E. Bar graphs in (B and E) represent mean ± SD of three biological replicates. In (C), bar graphs show mean ± SD from three independent sets, each with three biological replicates. Statistical significance was determined by an unpaired two-tailed Student's *t* test (*$p < 0.05$; **$p < 0.01$; ***$p < 0.001$; ns, not significant).

translation. Compared with the G-clade sequence, the Wuhan 5′UTR drove higher Nsp1 expression from the sgRep, which appeared to facilitate replication, leading to an increase in nucleocapsid (N) protein expression (Figure 2D). Enhanced translation was similarly observed in capped mRNAs encoding a stabilized BA.1 S(SA) vaccine antigen (Figure 2E). Minimal domain mapping experiments demonstrated that Wuhan strain gRNA-derived SL4.5–5 (ΔSL1–4) is sufficient to confer IRES activity in a conventional mRNA backbone (Figure 2F).

Together, these results demonstrate that the conserved C_{203} and C_{241} residues within the 5′–UUU(C)GU–3′ loop motif of SL5a and SL5b are indispensable for both efficient IRES-mediated and cap-dependent translation.

The SL4.5–5 element acts as a portable *cis*-acting module conferring IRES activity

Having identified the optimal SCoV2 SL4.5–5 element that confers cap-independent translation activity both at intergenic sites and the 5′ region of mRNAs, we next investigated its potential as a modular RNA element to enable dual translation initiation in synthetic mRNA constructs.

We first assessed whether the 175-nt SL4.5–5 (ΔSL1–4, Wuhan strain) could function as a 5′UTR to support cap-dependent translation of a vaccine antigen. Compared to the 301-nt Wuhan IRES, which exhibited efficiency equivalent to the human α-globin 5′UTR in cap-dependent translation (Figure S4A), SL4.5–5 alone showed reduced activity (Figure 3A). We then tested whether SL4.5–5 could confer IRES activity when fused downstream of cap-dependent 5′UTRs. Insertion of the SL4.5–5 element downstream of the 5′UTR of the human α-globin mRNA sequence (creating the hybrid "AS") markedly enhanced cap-independent expression of the BA.5 S(SA) antigen from uncapped mRNA (mRNA2). In contrast, the corresponding transcript lacking SL4.5–5 (mRNA1) produced only minimal antigen levels in both MAVS KO Huh7 and HEK293T cells (Figure 3B). A comparable enhancement by SL4.5–5 incorporation was also observed in mouse C2C12

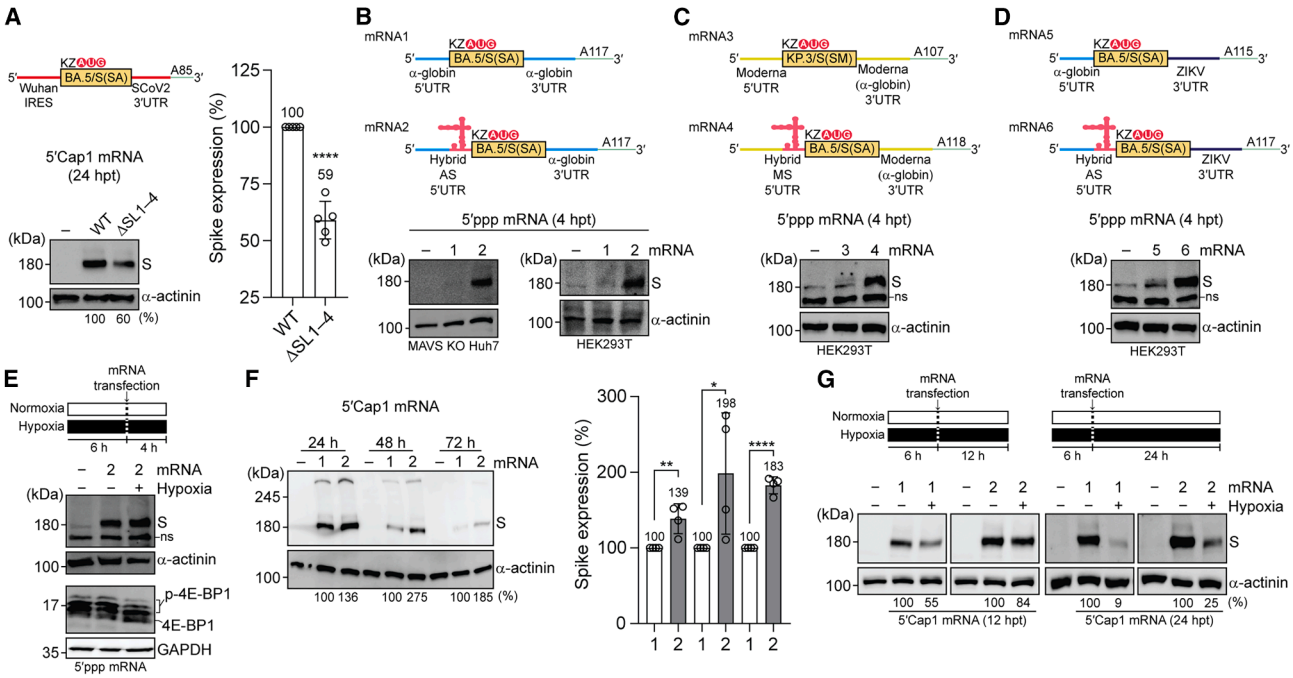

Figure 3. Positive impact of the SL4.5–5 IRES element on translation when placed downstream of heterologous 5′UTRs in cap-dependent mRNAs

(A) SL4.5–5 requires upstream SL1–4 for optimal antigen expression from capped mRNAs. (B–E) Schematic of uncapped mRNAs used to evaluate cap-independent capacity. Spike antigen expression was analyzed in MAVS-KO cells (B) or HEK293T cells (B–E) transfected with indicated uncapped mRNAs (5 μg per well in a six-well plate, Lipofectamine 2000) under normoxic (B–D) and/or hypoxic (E) conditions. (F) Kinetics of spike antigen expression in HEK293T cells transfected with capped mRNA1 or mRNA2 (1 μg, microfluidic LNP formulation). (G) Spike antigen expression following transfection with 0.5 μg mRNA-LNP under the indicated culture conditions. Data represent means ± SD from five biological replicates (A) and four biological replicates (F). Spike antigen expression level was analyzed as in Figure 1E. Statistical significance was determined by an unpaired two-tailed Student's *t* test (*$p < 0.05$, **$p < 0.01$, ****$p < 0.0001$).

myoblasts and DC2.4 dendritic cells, which represent the major cell populations likely translating mRNAs following intramuscular mRNA-LNP administration (Figure S4C). Similarly, insertion of SL4.5–5 downstream of the 5′UTR derived from the Moderna COVID-19 mRNA vaccine sequence generated a hybrid 5′UTR ("MS") that supported markedly higher cap-independent translation from uncapped mRNA (mRNA4) than its parental counterpart lacking SL4.5–5 (mRNA3) (Figure 3C).

To determine whether the function of SL4.5–5 depends on the α-globin 3′UTR present in mRNA2 and mRNA4, we replaced this element with the Zika virus (ZIKV) 3′UTR in uncapped mRNA1 and mRNA2, generating mRNA5 and mRNA6, respectively (Figure 3D). The hybrid "AS" 5′UTR in mRNA6 displayed robust IRES activity, confirming that the cap-independent translation driven by SL4.5–5 is independent of the 3′UTR context.

Notably, fusion of SL4.5–5 consistently converted uncapped conventional mRNAs (mRNA1, mRNA3, and mRNA5), which were otherwise non-functional or least-functional, into transcripts capable of IRES-mediated translation. Although SL4.5–5 enables cap-independent translation regardless of 3′UTR, translation efficiency varied by specific 5′ and 3′ combinations, with the strongest activity observed when SL4.5–5 was linked to the α-globin 5′UTR, as demonstrated by the order of translation efficiency: mRNA2 > mRNA6 > mRNA4 (Figure S4D). Moreover, among the capped mRNAs tested, the construct containing the hybrid 5′UTR "AS" (mRNA2) produced the highest level of spike antigen (Figure S4E), indicating its superiority in promoting translation under both capped and uncapped conditions.

We then focused on mRNA2 to further characterize its cap-independent translation capacity mediated by the IRES activity of SL4.5–5. Because uncapped mRNAs can undergo intracellular re-capping,[17] we assessed IRES activity under hypoxic conditions, which suppress cap-dependent translation. Expression of BA.5 S(SA) antigen from uncapped mRNA2 was maintained under hypoxia (Figure 3E), confirming effective cap-independent, IRES-mediated translation. Notably, capped mRNA2 drove approximately 2-fold higher and more sustained antigen expression than capped mRNA1 in HEK293T cells (Figure 3F), as well as murine cell lines C2C12 and DC2.4 (Figure S4F). In these cell types, capped mRNA4, which harbors the "MS" hybrid 5′UTR, showed a 1.8- to 3.3-fold increase in spike antigen expression relative to mRNA3 (Figure S4G). Although the SL4.5–5 incorporation enhanced the cap-dependent translation of mRNA1, neither mRNA1 nor mRNA2 reduced

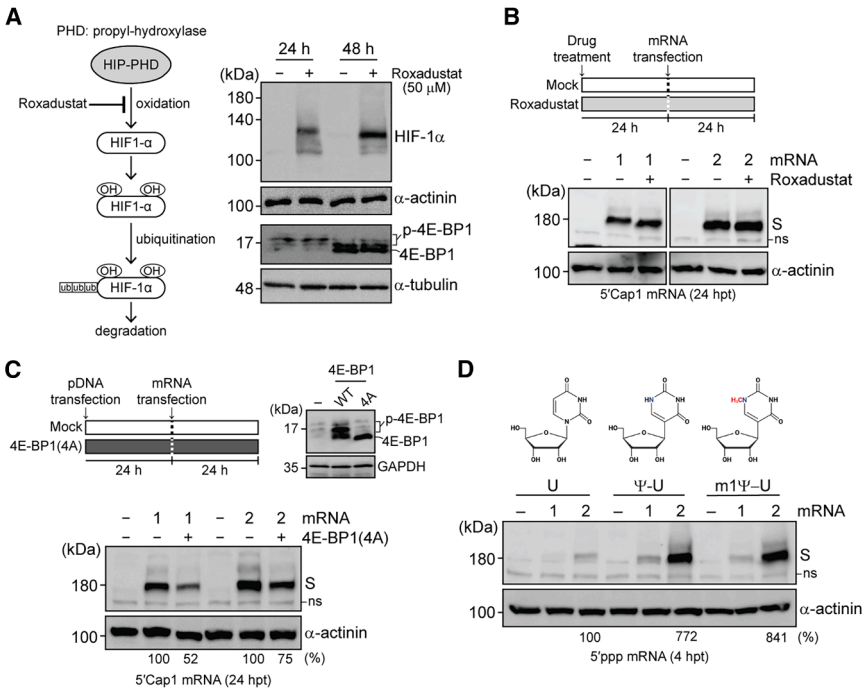

Figure 4. HIF-1α independence and resistance of the SL4.5–5 hybrid 5′UTR to dephosphorylated 4E-BP1, and its compatibility with modified uridines

(A) Stabilization of HIF-1α in HEK293T cells treated with the PHD inhibitor Roxadustat (50 μM) for 48 h, with no effect on 4E-BP1 phosphorylation status. (B) HIF-1α accumulation does not directly inhibit cap-dependent translation from mRNA1 (hypoxia-sensitive) or mRNA2 (hypoxia-resistant). Immunoblot analysis of spike antigen expression 24 h post-transfection of HEK293T cells with 1 μg microfluidic LNP-formulated mRNA, following Roxadustat (50 μM) or mock treatment. (C) The hybrid 5′UTR in mRNA2, which supports dual translation initiation, shows increased resistance to constitutively active, dephosphorylated 4E-BP1 compared to the mRNA1 5′UTR. Spike expression was analyzed 24 h post-transfection with 1 μg of microfluidic LNP-formulated mRNA following ectopic expression of wild-type or mutant 4E-BP1 in HEK293T cells. (D) Compatibility of SL4.5–5 IRES activity with modified uridines. Spike antigen expression level was analyzed as in Figure 1E.

reporter expression, suggesting that these constructs impose little to no translational burden in transfected cells (Figure S5). Moreover, SL4.5–5-mediated translation enhancement conferred strong resilience to translational inhibition. Under hypoxic conditions, capped mRNA2 exhibited substantially higher antigen expression than capped mRNA1 (Figure 3G).

Together, these findings establish that the SL4.5–5 element functions as a portable *cis*-acting module that confers IRES activity on otherwise cap-dependent 5′UTRs. Its inclusion enables dual translation initiation, thereby extending expression kinetics and preserving protein synthesis under hypoxic conditions.

The IRES activity of SL4.5–5 is independent of HIF-1α and compatible with modified uridines

The transcription factor HIF-1α is multifunctional, forming a DNA-binding heterodimer with constitutively expressed HIF-1β and dynamically localizing between the cytoplasm and nucleus.[18] Since IRES activity can be influenced by RNA-binding proteins,[19,20] we investigated whether the IRES function of the SL4.5–5 module is regulated by the nucleic-acid-binding activity of HIF-1α, which is stabilized under hypoxia via the inhibition of HIF-prolyl hydroxylase (HIF-PHD). Treatment of HEK293T cells with Roxadustat, an HIF-PHD inhibitor, led to robust stabilization of HIF-1α, which was maintained without signal attenuation for up to 48 h (Figure 4A). Notably, Roxadustat treatment did not alter 4E-BP1 phosphorylation status, but at later time points, most 4E-BP1 appeared hypophosphorylated, likely due to increased cell density suppressing mTORC1 activity.[21]

Importantly, elevated HIF-1α levels did not alter spike antigen expression from capped mRNA1 or mRNA2 (Figure 4B), indicating that the IRES activity of SL4.5–5 is not dependent on HIF-1α by itself or its downstream transcriptional activation pathways. Rather, SL4.5–5 conferred cap-independent translation capacity in a manner resistant to inhibition by the constitutively active 4E-BP1(4A) mutant, which carries Ala substitutions at four regulatory phosphorylation sites (T37A, T46A, S65A, and T70A)[22] (Figure 4C). These findings reinforce that SL4.5–5 bypasses canonical cap-dependent control mechanisms.

We next investigated whether the incorporation of modified uridines, a hallmark of current mRNA vaccines,[1] is compatible with SL4.5–5 function. *In silico* modeling predicted that pseudouridine (Ψ-U) incorporation would not alter the SL4.5–5 secondary structure (Figure S6), despite its known ability to stabilize base-pairing interactions.[23] To validate this experimentally, we synthesized uncapped mRNA1 and mRNA2 containing either natural uridine (U), Ψ-U, or N1-methylpseudouridine (m1Ψ-U) and compared their ability to support cap-independent translation. In all cases, SL4.5–5 enhanced cap-independent translation when linked to the downstream of the mRNA1 5′UTR (Figure 4D).

Moreover, modified uridines markedly enhanced spike expression. Specifically, Ψ-U and m1Ψ-U increased protein output from uncapped mRNA2 by 772% and 841%, respectively. To confirm that these differences arose from mRNA modifications rather than from variations in RNA quality, we compared the integrity of mRNA2 variants containing natural or modified uridines. All variants showed

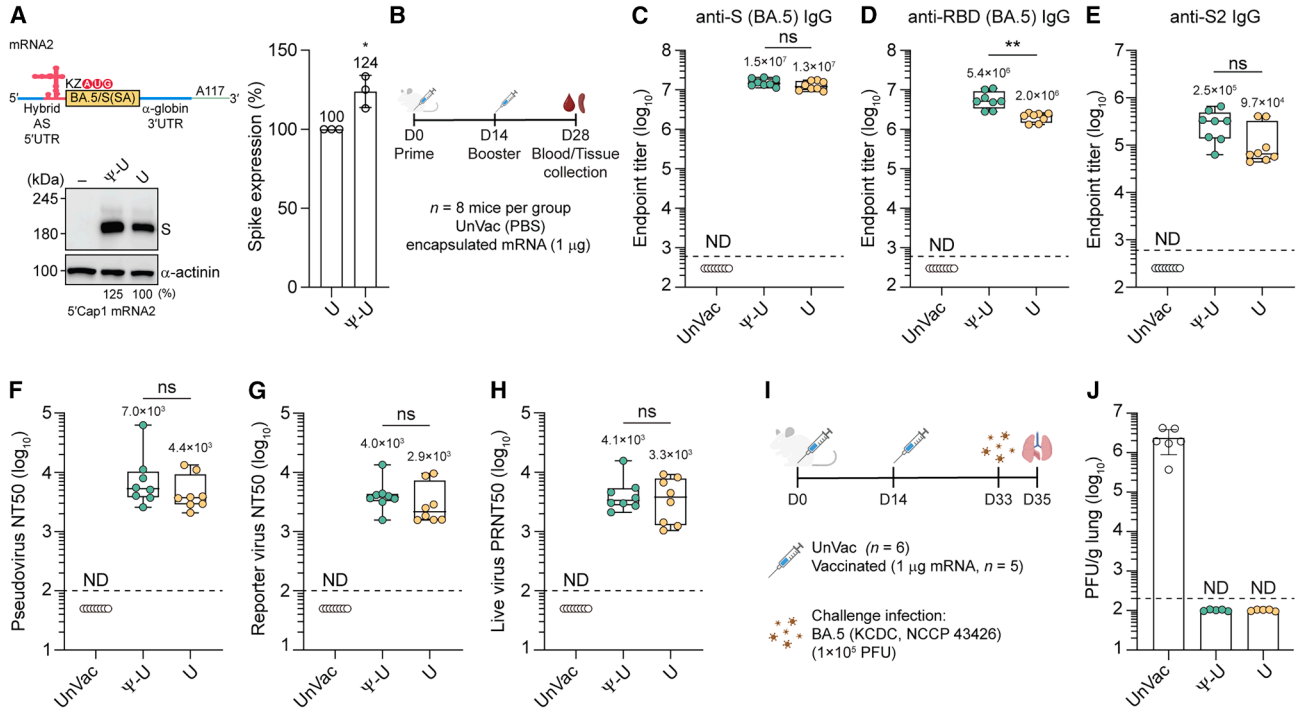

Figure 5. Immunogenicity and protective efficacy of unmodified and Ψ-uridine-modified capped mRNA2-LNP vaccines targeting Omicron BA.5

(A) Immunoblot analysis of Omicron BA.5 spike antigen expressed from unmodified and Ψ-U-modified capped mRNA2. Spike antigen expression level was analyzed as in Figure 1E. Data represent means ± SD from biological triplicates. (B) Immunization and sample collection schedule. Female BALB/c mice (7–8 weeks old) were immunized twice at a 2-week interval with PBS (UnVac) or capped, U- or Ψ-U-incorporated mRNA2 (1 μg) formulated in LNPs ($n = 8$ per group). Blood was collected 2 weeks post-boost. (C–E) Serum IgG geometric mean endpoint titers (GMT) against Omicron BA.5 full-length spike protein (C), receptor-binding domain (RBD) (D), and S2 subunit (E). (F–H) Neutralizing antibody titers (NT50) measured by pseudovirus neutralization assay (F), reporter-expressing recombinant SCoV2 assay (G), and live virus plaque reduction assay (H). Each data point represents NT50 values from biological triplicates (F) or duplicates (G and H). (I and J) Viral challenge experimental schema (I) and lung viral loads (J) measured by plaque assay 2 days post-intranasal challenge with 1×10^5 PFU of Omicron BA.5 in immunized mice. Each data point represents the mean of biological duplicates. Data are presented as mean ± SD. Boxplots show the median (line), interquartile range (box), and individual values. GMT values are indicated above the boxes. Values below the detection limit (ND) were assigned half the limit of detection (LOD) for visualization. Statistical significance was assessed by an unpaired two-tailed Student's *t* test (**$p < 0.01$; ns, not significant).

comparable synthesis yields and integrity (Figure S7A), with modified mRNAs exhibiting faster migration on denaturing agarose gels due to their more compact structure. No longer-than-full-length or early-terminated abortive transcripts were detected (Figures S7B). We also quantified double-stranded RNA (dsRNA) levels to rule out innate immune activation by impurities. Modified mRNAs showed lower dsRNA levels than unmodified ones (Figures S7C and S7D), likely due to reduced binding affinity of the K1 monoclonal antibody to m1Ψ-U-containing mRNAs.[24,25] Nevertheless, all dsRNA impurity levels were below 0.05% (w/w) (Figures S7C and S7D). Supplementary analysis further confirmed elevated spike expression from modified uncapped mRNAs (Figure S7E), demonstrating that the enhanced antigen expression resulted from uridine modifications, which enhance mRNA stability.

Together, these findings demonstrate that the SL4.5–5 module functions independently of HIF-1α per se or HIF-1α signaling, while being fully compatible with modified nucleotides. This versatility enables potent cap-independent translation without compromising canonical translation pathways, supporting the utility of SL4.5–5-based hybrid 5′UTRs for robust mRNA expression across diverse cellular environments.

Immunogenicity and protective efficacy of unmodified mRNA2-LNP vaccines against Omicron BA.5

Building on the compatibility of modified uridines with SL4.5–5 IRES activity and enhanced antigen expression observed with capped mRNA2, we evaluated the immunogenicity of an unmodified mRNA2-LNP vaccine harboring the AS hybrid 5′UTR. In capped transcript context, Ψ-U mRNA2-LNP control showed ~24% higher BA.5 S(SA) antigen expression in HEK293T cells compared to the unmodified mRNA2 (Figure 5A).

BALB/c mice were immunized twice at a 2-week interval with 1 μg of each formulation (Figure 5B). Both unmodified and Ψ-U mRNA2-LNP vaccines induced high BA.5 S-binding immunoglobulin G (IgG) titers (>10^7 reciprocal endpoint; Figure 5C). Ψ-U incorporation significantly boosted RBD-specific IgG titers 2.7-fold

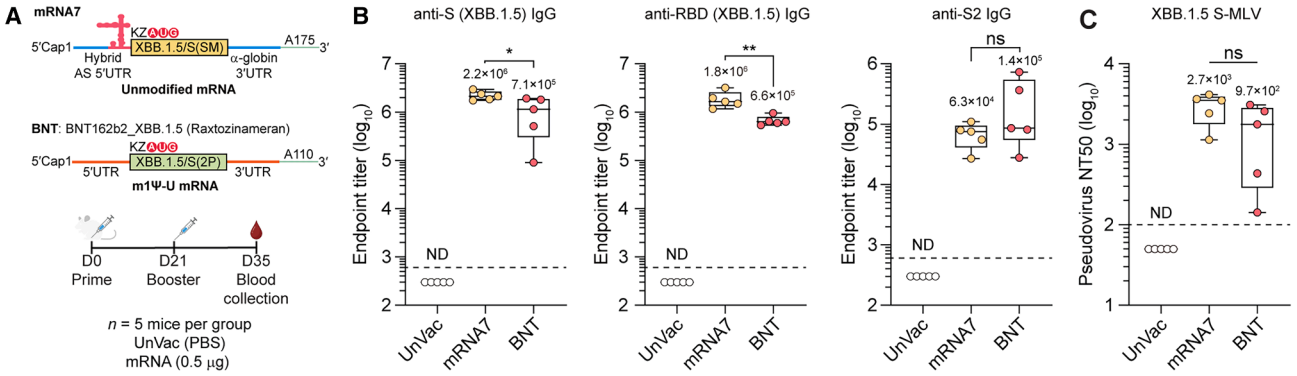

Figure 6. Comparative immunogenicity of unmodified mRNA7 and modified BNT162b2 vaccines targeting Omicron XBB.1.5

(A) Schematic of mRNA7 and raxtozinameran (BNT162b2_XBB.1.5) constructs and immunization/sample collection timeline. Female BALB/c mice (7–8 weeks old) were immunized twice at a 3-week interval with PBS (UnVac), 0.5 μg of unmodified mRNA7-LNP, or raxtozinameran ($n = 5$ per group). (B) Serum IgG geometric mean titers (GMT) measured 2 weeks post-boost against Omicron XBB.1.5 full-length spike protein, RBD, or S2 subunit. (C) Neutralizing antibody titers (NT50), determined by pseudovirus neutralization assay. Each data point represents NT50 values from biological triplicates. Dotted lines indicate the limit of detection (LOD). Non-detected (ND) antibody levels were assigned half the LOD for graphical representation. Statistical significance was determined by an unpaired two-tailed Student's *t* test (*$p < 0.05$; **$p < 0.01$; ns, not significant).

($p = 0.0027$; Figure 5D), while both groups showed robust S2-specific responses (Figure 5E), potentially contributing to cross-variant protection.[26]

Cellular immunity, assessed by IFN-γ ELISpot, revealed ∼2,000 spot-forming units per million splenocytes in both cohorts, indicating strong S-protein-specific T cell responses (Figure S8A). Neutralizing antibody titers against BA.5 exceeded a geometric mean titer (GMT) of 10^3 across pseudovirus (Figure 5F), reporter virus (Figure 5G), and authentic virus (Figure 5H) neutralization assays, with no significant differences between modified and unmodified mRNA vaccines.

Upon intranasal challenge with 10^5 PFU of BA.5, both vaccinated groups showed complete protection, with no detectable infectious virus in lungs (Figures 5I and 5J) and marked reductions in viral RNA (Figure S8B). Immunohistochemistry revealed viral N protein only in sham controls, which also showed alveolar damage on H&E staining (Figure S8C). Vaccinated mice showed minimal pathology and notable $CD3^+$ T cell infiltration, suggesting rapid local T cell activation as a key factor in viral clearance.

Both Ψ-U and natural U-containing mRNAs (0.5 μg in HEK293T cells; 0.25 or 1 μg in BALB/c mice) elicited no noticeable inflammatory immune responses. In contrast, intramuscular administration of 10 μg of either mRNA formulation induced marked elevations in the proinflammatory cytokines interleukin (IL)-6, interferon alpha (IFN-α), and IFN-γ, while IL-1β and tumor necrosis factor α (TNF-α) levels remained unchanged (Figure S9).

Comparison of unmodified mRNA7-LNP and m1Ψ-U-modified BNT162b2/raxtozinameran against Omicron XBB.1.5

We next examined whether the AS hybrid 5′UTR could confer comparable efficacy to unmodified COVID-19 vaccine mRNA relative to m1Ψ-U modified mRNA. To test this, we constructed RNA7 encoding a fusion-defective XBB.1.5 Spike (SM) antigen with R685S and R815M substitutions, flanked by the AS hybrid 5′UTR and an α-globin 3′UTR with a 175-nt poly(A)-tail. We compared this Omicron XBB.1.5-targeting mRNA7-LNP vaccine with the clinically approved m1Ψ-U-modified BNT162b2 vaccine targeting the same variant (raxtozinameran), which encodes a prefusion-stabilized XBB.1.5 S(2P) antigen (Figure 6A). Both LNP-formulated vaccines contained intact, single-species mRNA (Figure S10A) and expressed their respective antigens with distinct cleavage profiles *in vitro* (Figure S10B).

BALB/c mice immunized twice, three weeks apart, with 0.5 μg of each vaccine mounted strong humoral immune responses. Notably, mRNA7 elicited significantly higher IgG titers than raxtozinameran (3.1-fold increase in S-binding IgG, $p = 0.0280$; 2.7-fold increase in RBD-binding IgG, $p = 0.0092$; Figure 6B). Neutralizing antibody titers against pseudovirus exceeded 10^3 GMTs in both groups (Figure 6C). Despite lacking modified uridines and using a sub-microgram dose, mRNA7 elicited comparable or superior antigen-specific IgG and neutralization titers, with all mice achieving NT50 values greater than 10^3. This potent immunogenicity persisted across all tested doses (0.25 μg, 0.5 μg, and 1 μg), yielding anti-XBB.1.5 neutralizing antibody titers greater than 10^3 GMTs, in both PNA and PRNT assays (Figures S11A–S11C). These findings demonstrate that unmodified mRNA with the SL4.5–5 hybrid 5′UTR elicits humoral immunity that matches or exceeds the levels achieved by the m1Ψ-U-modified raxtozinameran.

Omicron variant (B.1.1.529 lineage), particularly those harboring extensive RBD mutations (Figure S11D), evade immunity induced by ancestral S antigens.[27,28] Cross-neutralization testing against diverse XBB subvariants (XBB.1.16, EG.5, and XBB.2.3.2) and

BA.2.86 revealed substantially reduced neutralization of BA.2.86 (Pirola), a BA.2 sublineage with more than 30 spike amino acid substitutions relative to XBB.1.5,[29] compared with the other tested strains (Figures S11E–S11H). These results highlight the rapid antigenic diversification within Omicron lineages and the need for iterative antigen updates to maintain neutralization breadth in the next-generation mRNA vaccines.

DISCUSSION

Beyond infectious disease vaccines, the mRNA platform offers broad applications, including therapeutic cancer vaccines, protein replacement, stem cell reprogramming, and next-generation cell therapies.[1,30] However, conventional mRNA modalities remain constrained by their reliance on cap-dependent translation, which can be suppressed in various *in vivo* environments that restrict cap-dependent translation. Overcoming this limitation can improve the efficacy of both preventive and therapeutic mRNA applications. Cap-independent initiation offers a promising alternative. IRES elements, found in diverse viral and cellular RNAs, allow protein synthesis to proceed even when canonical cap-dependent initiation is inhibited.[4,5,31] Notably, circular RNA (circRNA)-based vaccines currently under development exploit IRES-driven mechanisms to bypass the dependence on the 5′ cap.[32] However, in general, unmodified circRNAs show lower translation efficiency than conventional linear mRNAs, while some recently reported circRNAs incorporating IRES elements from human rhinovirus B and enterovirus B supported more sustained protein production over time, making them attractive platforms for certain therapeutic applications requiring prolonged antigen or protein expression.[33,34]

In this study, we sought to address this challenge by designing a hybrid 5′UTR that engages both cap-dependent and cap-independent translation mechanisms to maximize translation efficiency. Our strategy harnessed a unique *cis*-acting RNA module derived from the SCoV2 gRNA 5′UTR. Located within SL4.5–5, this element conferred IRES activity, a property absent in sgRNAs, which are relatively more abundant than gRNA. Although both SCoV2 gRNA and sgRNAs are capped by the viral RNA-dependent RNA polymerase (Nsp12) complex,[15] exclusive reliance on cap-dependent initiation would not be optimal for viral translation. Under cap-dependent translation-restrictive conditions, the genomic 5′UTR likely supports cap-independent initiation to sustain viral protein synthesis and replication efficiency.

During SARS-CoV-2 infection, the virus encounters cap-dependent translation-unfavorable stress conditions. Hypoxia, for instance, is a hallmark of cytokine-storm-damaged tissues that can reduce canonical translation.[31] Furthermore, SCoV2 infection induces the generation of reactive oxygen species (ROS) in lung tissue, contributing to oxidative stress, DNA damage, and cellular senescence.[35] Additionally, starvation of nutrients such as amino acids and glucose, as well as low ATP levels in virus-infected cells, can lead to inhibition of the mTOR pathway,[36] thereby suppressing cap-dependent translation through dephosphorylation and increased binding of 4E-BP1 to eIF4E. Lastly, cap-dependent translation can also be inhibited by proteolytic cleavage of eIF4G by the viral protease Nsp5, as we (Figure S12) and others[12] have observed.

Our data provide direct evidence that the SCoV2 gRNA 5′UTR harbors IRES activity, specifically conferred by SL4.5–5. This feature enables viral protein synthesis under conditions hostile to canonical cap-dependent translation initiation, highlighting SCoV2's evolutionary adaptation that promotes viral replication in hypoxic or stressed host environments. Remarkably, among tested variants, the ancestral Wuhan SL4.5–5 element conferred superior IRES activity compared to G-clade and Delta sequences (Figure 2), underscoring the evolutionary divergence of this structural module since SCoV2 spilled over into the human population.

From a physiological perspective, the SCoV2 IRES activity likely facilitates the translation of the first viral ORF (ORF1a/b), including Nsp1. Nsp1 is known to help the ribosome selectively translate SCoV2 gRNA and sgRNA, both of which contain SL1, while suppressing cellular mRNAs that are also similarly capped at the 5′-end.[37] A recent study also supports the idea that Nsp1 is necessary for the selective translation of viral RNA over host mRNA in an EIF1/1A-dependent manner.[38] Our findings explain how SCoV2 could prioritize its own protein production during infection, especially under conditions where cap-dependent translation is suppressed, and viral mRNAs compete with cellular mRNAs for the translation machinery. In this context, we propose that SCoV2 uses the IRES activity provided by the SL4.5–5 region to regulate the translation of viral Nsps, including Nsp1 and other components of the replicase complex,[39] thereby supporting viral genome replication.

Our findings show that the SL4.5–5 module functions as an effective IRES element, enabling mRNA translation to continue efficiently even when typical cap-dependent translation is blocked under stress conditions such as hypoxia. Additionally, it not only enables robust translation from capless mRNAs but also boosts overall protein production beyond that of standard capped mRNAs lacking this module under normal, non-stressed, or normoxic conditions. Incorporating the SL4.5–5 module into mRNA vaccines could therefore substantially enhance antigen expression and vaccine effectiveness across a wide range of physiological environments, including but not limited to challenging situations where traditional cap-dependent translation is limited.

Building on this insight, we used the SL4.5–5 module, specifically the ancestral Wuhan strain sequence, which exhibits higher IRES activity than later variants, to engineer hybrid 5′ UTRs that support dual-mode translation initiation. These hybrid 5′UTRs showed robust cap-dependent and IRES-mediated translation, outperforming conventional mRNA vaccine 5′UTRs. Notably, our findings reveal a novel role for the SL4.5–5 element in enhancing cap-dependent translation, provided it is positioned downstream of short, functional 5′UTRs (e.g., the 34-nt α-globin [Figure S6A] or the

57-nt Moderna mRNA-1273 UTR) (Figures 3A, 3F, and S4G). This enhancement appears to mirror the requirement for upstream SLs observed in the capped SCoV2 gRNA 5′UTR context (Figure 3A). We propose that this effect occurs via ribosome shunting, in which upstream-structured SLs in conjunction with the 5′cap recruit the 40S complex and transfer it directly to the translation initiation sites downstream of the engineered SL4.5–5 long-stem (Figure S6) or the AUG embedded within the SL5 stem (nts 266–268) (Figure 1B).

Such shunting would facilitate ribosome positioning at these start sites without requiring the energy-intensive scanning of the stable SL5 stem by the eIF2A helicase. Mechanistically, direct 18S rRNA base-pairing[40] is unlikely to be involved, as no complementary sites are present upstream of the AUG site in either the SCoV2 gRNA 5′UTR or our engineered "AS" and "MS" hybrid 5′UTR (Figures 3B and 3C). Thus, a plausible mechanism for this enhanced efficiency via coupled cap/IRES initiation is ITAF (IRES-*trans*-acting factor)-mediated ribosome shunting, which allows the translation complex to bypass highly structured IRES elements. Given the multiple SCoV2 5′UTR-binding proteins identified by Flynn et al.,[41] future studies will focus on identifying the specific ITAFs that enable this dual translation initiation across both capped and uncapped mRNA contexts. Regardless of the underlying mechanisms, we establish that the SL4.5–5 element is a portable *cis*-acting module that confers IRES activity on otherwise cap-dependent 5′UTRs. Its inclusion enables dual translation initiation, thereby extending expression kinetics and preserving protein synthesis under conditions that suppress cap-dependent translation. This functionality was maintained regardless of whether the mRNA contained modified uridines.

While modified uridines enhance mRNA stability and increase translation efficiency, certain modifications, such as m1Ψ-U, have been linked to ribosome-stalling-mediated frameshifting in specific sequence contexts and decreased translational fidelity through abnormal decoding.[42,43] We demonstrated that unmodified uridine-containing mRNA vaccines were just as effective as their modified versions in eliciting humoral and cellular immunity (Figures 5, 6, and S9). In head-to-head comparisons, unmodified uridine-based Omicron XBB.1.5 mRNA-LNP vaccines induced neutralizing antibody responses comparable to those generated by the m1Ψ-U-incorporated Pfizer/BioNtech mRNA vaccine formulation. Therefore, the SL4.5–5-based hybrid UTR not only enables durable antigen expression even under challenging cellular conditions but also supports the use of unmodified uridines, thereby reducing the risk of mistranslation associated with nucleoside modifications.

As our results and others have demonstrated, intramuscular (i.m.) administration of COVID-19 mRNA-LNP vaccines elicits strong systemic IgG responses that can be actively transported into the lungs via the neonatal Fc receptor (FcRn). This translocation can enhance humoral protection against SARS-CoV-2 in the lower respiratory tract despite limited mucosal immunity.[44–46] Such a mechanism aligns with early clinical interventions during the pandemic, where passive immunization strategies, including intravenous monoclonal antibodies, were used to provide immediate protection against severe COVID-19.[47]

In summary, this study introduces SL4.5–5-derived hybrid 5′UTRs as a versatile tool for mRNA design, uniquely enabling both cap-dependent and IRES-mediated cap-independent translation initiation. This dual functionality maximizes gene expression across various physiological conditions, offering advantages beyond what traditional linear-capped mRNA or circular RNA approaches can achieve. The demonstrated compatibility of this platform with both modified and unmodified uridines, without sacrificing vaccine efficacy, further enhances its translational potential. These findings strongly support advancing SL4.5–5-based hybrid UTR mRNA technologies into preclinical and clinical evaluations across multiple fields, including vaccines, protein replacement therapies, and engineered cell therapies.

MATERIALS AND METHODS

Plasmids and reagents

The SCoV2 sgRep was constructed using pBAC-SARS-CoV-2/YS006, a full-length cDNA clone of the G-clade SCoV2 strain YS006.[48] A more detailed description of the sgRep construct is provided in the supplemental information.

Plasmid DNAs used as templates for *in vitro* transcription of S-protein-encoding mRNAs were designed to allow co-transcriptional capping with CleanCap AG (3′ OMe) (TriLink, San Diego, CA, USA; cat. no. N-7413). Two template plasmids used for the synthesis of mRNA transcripts encoding a 20-nt-long poly(A) tail (Figure 2E) contained an HDVr sequence at the 3′ end, while transcripts with longer poly(A) tails were generated from templates containing a poly(dT) stretch.

pDual-IRES encoding *Renilla* luciferase (Rluc) and Firefly luciferase (Fluc), by cap-dependent translation and IRES-mediated translation, respectively, was described previously.[20] Various SCoV2 genome-derived *cis*-acting sequences were inserted in place of the HCV IRES sequence using the In-Fusion HD cloning kit (Takara Bio, Kusatsu, Shiga, Japan; cat. no. 638947) to test for their IRES activity at an intergenic site.

Human-codon-optimized SCoV2 protein-coding cDNAs were designed based on publicly available sequence (Wuhan-Hu-1 reference strain, GeneBank: YP_009724390.1) and synthesized by Twist Bioscience (South San Francisco, CA, USA) or Bionics Inc. (Seoul, South Korea).

The expression plasmid for human 4E-BP1 was constructed as follows. Total RNA was extracted from HEK293T cells using TRIzol reagent (Invitrogen, Waltham, MA, USA; cat. no. 15596018), and reverse transcription targeting the 4E-BP1 gene (NCBI GeneBank: NM_004095.4) was performed using ImProm-II Reverse Transcriptase (Promega, Madison, WI, USA; cat. no. A3803) and a reverse

primer 5′-TTA AAT GTC CAT CTC AAA CTG TGA CTC TTC-3′. The resulting cDNA encoding 4E-BP1 was PCR-amplified and cloned into the pcDNA3.1 vector (Invitrogen; cat. no. V79020) using the In-Fusion HD Cloning Kit (Takara Bio).

Single residue changes were introduced into plasmids using the QuikChange II XL Site-Directed Mutagenesis Kit (Agilent, Santa Clara, CA, USA; cat. no. 200521). Plasmids with multiple residue changes or deletions were generated using the In-Fusion HD Cloning Kit (Takara Bio).

Lipofectamine 2000 (Invitrogen; cat. no. 11668019) was used for plasmid and uncapped mRNA transfection. Roxadustat (FG-4592) was purchased from MedChemExpress (Monmouth Junction, NJ, USA; cat. no. HY-13426).

Cell culture and virus

HEK293T, BHK21, C2C12, DC.2.4, and VeroE6 cells were obtained from the American Type Culture Collection (ATCC, Rockville, MD, USA). VeroE6 cell line stably expressing hTMPRSS2 (VeroE6/TMPRSS2) was a gift from Dr. Seong-Jun Kim (Korea Research Institute of Chemical Technology, KRICT, Daejeon, South Korea). VeroE6 cell line stably expressing both human TMPRSS2 and ACE2 (VeroE6-TMPRSS2-T2A-ACE, hereafter referred to as VeroE6/A2-T2) was obtained from BEI Resources, NIAID, NIH (cat. no. NR-54970). The MAVS-knockout Huh7 cell line (Huh7/MAVS KO) was previously generated using the CRISPR-Cas9 system.[49] All cell lines used in this study were regularly tested for mycoplasma contamination via PCR analysis of the cell culture supernatant, following previously established protocols.[50]

HEK293T, BHK21, C2C12, DC.2.4, VeroE6, and Huh7/MAVS KO cells were maintained in Dulbecco's modified Eagle medium (DMEM) supplemented with 10% fetal bovine serum (FBS), 100 U/mL penicillin, and 100 μg/mL streptomycin (complete medium), at 37°C in a humidified incubator with 5% CO_2. VeroE6/TMPRSS2 and VeroE6/A2-T2 cells were cultured in complete medium supplemented with 150 μg/mL hygromycin and 10 μg/mL puromycin, respectively. All stably selected cell lines were passaged once in antibiotic-free complete medium prior to experimental plating.

Cells subjected to hypoxic conditions were cultured in a hypoxic incubator at 1% O_2 concentration using Forma Series II 3110 Water-Jacketed CO_2 Incubator (Thermo Fisher Scientific, Waltham, MA, USA; cat. no. 3131).

The patient-derived SCoV2 strain used in challenge infection studies (Omicron BA.5, NCCP 43426) was obtained from the National Culture Collection for Pathogens (NCCP), a division of the Korea Centers for Disease Control and Prevention (KCDC, Osong, South Korea). The virus was propagated in VeroE6/TMPRSS2 cells, and viral titers were determined by plaque assay using the same cell line, as previously described.[51] All experiments involving live SCoV2 infection with patient-isolated or plasmid-rescued recombinants were conducted in a biosafety level 3 (BSL-3) facility at the Avison Biomedical Research Center (ABMRC), Yonsei University College of Medicine.

In vitro transcription and mRNA transfection

Template plasmids encoding mRNAs with a 3′ HDVr sequence were linearized with SacII, while plasmids encoding mRNAs with a poly(A) run-off tail were linearized with BbsI. Linearized plasmids were purified using the Gel Extraction Kit (Bionics; cat. no. BNROP-0020) and used as templates for *in vitro* transcription with the MEGAscript T7 Transcription Kit (Invitrogen; cat. no. AMB13345). When indicated, Ψ-UTP (TriLink; cat. no. N-1019) or N1-methyl-Ψ-UTP (TriLink; cat. no. N-1081) was substituted for UTP to generate modified mRNAs. The integrity of transcribed mRNAs was assessed by electrophoresis on a 0.7% formaldehyde-denaturing agarose gel and stained with ethidium bromide.

Co-transcriptional capping was performed by including CleanCap AG (3′ OMe) (TriLink; cat. no. N-7413) in the *in vitro* transcription reaction to generate 5′-capped (Cap1) mRNAs. Uncapped mRNAs bearing a 5′-triphosphate end were transfected into cells using Lipofectamine 2000 (Invitrogen), while 5′-capped mRNAs were transfected using either Lipofectamine 2000 or a laboratory-prepared lipid nanoparticle (LNP) formulation.

The lab-made lipid mix consisted of ionizable lipid SM-102 (MedChemExpress; cat. no. HY-134541), cholesterol (Sigma-Aldrich, St. Louis, MO, USA; cat. no. C8667), distearoylphosphatidylcholine (DSPC) (Avanti Polar Lipids, Alabaster, AL, USA; cat. no. 85030), and PEG2000-DMG (Avanti Polar Lipids; cat. no. 88051P), mixed in a molar ratio of 50:10:38.5:1.5, respectively. The lipids were formulated with mRNA in citrate buffer (pH 4) at an N:P ratio of 12.5:1.

SCoV2 subgenomic replicon assay

The SCoV2 sgRep RNA was synthesized *in vitro* using T7 RNA polymerase and co-transcriptionally capped with CleanCap AU (TriLink; cat. no. N-7114). HEK293T cells seeded in six-well plates were transfected with 1 μg of *in vitro*-transcribed replicon RNA per well using a laboratory-formulated lipid mix transfection reagent. At indicated time points post-transfection, cells were lysed with Glo Lysis Buffer (Promega; cat. no. E2661) for subsequent luciferase assay and immunoblotting.

NanoLuc luciferase activity was measured using the Nano-Glo Luciferase Assay System (Promega; cat. no. N1120) according to the manufacturer's protocol. Briefly, harvested cell lysates were clarified by centrifugation at 13,000 × g for 15 min at 4°C to remove cellular debris, and 50 μL of the supernatant was used for the assay. Relative light units (RLU) were quantified using a GloMax Navigator Microplate Luminometer (Promega). RLU values were normalized to total protein concentration, as determined by the Bradford assay.

Immunoblotting

Cells were lysed in RIPA buffer (150 mM NaCl, 1.0% NP-40, 0.5% sodium deoxycholate, 0.1% SDS, 50 mM Tris-HCl, pH 8.0)

supplemented with a protease inhibitor cocktail and, when detecting phosphorylated 4E-BP1, a phosphatase inhibitor (Thermo Fisher Scientific; cat. no. A32957). Lysates were clarified by centrifugation at 13,000 × g for 15 min at 4°C. Proteins were resolved by SDS-PAGE and transferred onto a PVDF membrane (GE Healthcare Life Sciences, Chicago, IL, USA; cat. no. 10600023). Membranes were blocked with 5% bovine serum albumin and incubated with the appropriate primary and secondary antibodies. When applicable, the intensity of the target protein band was quantified using ImageJ. The relative intensity (expressed as a percentage) of each sample was indicated below the corresponding blot, with the intensity of the reference sample set to 100%. Antibody probes used in immunoblotting are detailed in the supplemental information.

Dual-IRES plasmid luciferase assay

HEK293T cells seeded in six-well plates were transfected with 500 ng per well of the pDual-IRES using Lipofectamine 2000 (Invitrogen), following the manufacturer's instructions. At 24 or 48 h post-transfection, cells were lysed in Glo Lysis Buffer (Promega; cat. no. E2661), and the lysates were clarified by centrifugation at 13,000 × g for 15 min at 4°C to remove cellular debris. Seventy-five microliters of the resulting clarified lysate was used for luciferase measurement using the Dual-Glo Luciferase Assay System (Promega; cat. no. E2940), according to the manufacturer's protocol. Luminescence was recorded with a GloMax Navigator Microplate Luminometer (Promega). IRES activity was quantified as the ratio of Firefly luciferase RLU to *Renilla* luciferase RLU.

mRNA-LNP vaccine formulation

mRNA-LNP formulation for animal experiments was performed using the NanoAssemblr Spark system (Precision Nanosystems, Vancouver, Canada). Briefly, a lipid mixture consisting of ionizable lipid ALC-0315 (MedChemExpress; cat. no. HY-138170), cholesterol (Sigma-Aldrich; cat. no. C8667), helper lipid distearoylphosphatidylcholine (DSPC) (Avanti Polar Lipids, Alabaster, AL, USA; cat. no. 85030), and PEG-conjugated lipid ALC-0159 (MedChemExpress; cat. no. HY-138300) was prepared at a molar ratio of ALC-0315:DSPC:cholesterol:ALC-0159 = 46.3:9.4:42.7:1.6. The lipid mixture was combined with mRNA in citrate buffer (pH 4) at a nitrogen-to-phosphate (N:P) ratio of 6:1. The resulting mRNA-LNPs were dialyzed overnight against phosphate-buffered saline (PBS) containing 8% sucrose, as previously described.[52]

The particle size (100–140 nm) and uniformity (polydispersity index <0.2) of the mRNA-LNPs were assessed by dynamic light scattering using a particle size analyzer (ELSZ-1000, Otsuka Electronics, Osaka, Japan). Encapsulation efficiency, ranging from 70% to 80%, was determined using the Quant-iT RiboGreen RNA Assay Kit (Invitrogen; cat. no. R11490), as previously described.[53]

The Omicron XBB.1.5-adapted BNT162b2 vaccine (raxtozinameran; lot no. HH1301) was provided by Pfizer-BioNTech through the KCDC. These vaccine doses, originally procured by KCDC for the National Vaccination Program, were nearing expiration and provided—with the manufacturer's approval—for research and development purposes.

Animal experiments

All animal experiments were conducted in accordance with the guidelines of the Korean Food and Drug Administration. Experimental procedures were reviewed and approved by the Institutional Animal Care and Use Committee (IACUC) of the Yonsei Laboratory Animal Research Center (Permit numbers: IACUC-A-202203-1427-03 and IACUC-A-202311-1765-03). At the end of each experiment, mice were euthanized by CO_2 inhalation.

BALB/c mice (female, 7–8 weeks old) were immunized via intramuscular injection of 50 μL mRNA-LNP into the ipsilateral hindlimb for prime-boost vaccination, using an insulin syringe (BD, Franklin Lakes, NJ, USA; cat. no. 328868). Blood samples were collected either by tail-clip bleeding or by cardiopuncture. The collected blood was allowed to clot for 30 min at room temperature, then centrifuged at 6,000 × g for 25 min to obtain serum. Mouse sera were heat-inactivated by incubation at 50°C for 30 min prior to use.

IgG ELISAs

SCoV2 S-protein-binding IgGs were detected via ELISA. A detailed procedure is described in the supplemental information.

Neutralizing antibody titration

Pseudovirus neutralization assay (PNA), reporter virus neutralization assay (RVNA), and live virus plaque reduction neutralization (PRNT) were employed to measure neutralization antibody titers. A detailed procedure is provided in the supplemental information.

Challenge infection

A vaccine efficacy study using BALB/c mice was conducted in a biosafety level 3 (BSL-3) facility at the Avison Biomedical Research Center (ABMRC), Yonsei University College of Medicine. The study was approved under Institutional Biosafety Committee (IBC) permit number A-202009-260-01, and all animal experiments involving SCoV2 were conducted in accordance with protocols approved by the IACUC at Yonsei University College of Medicine (Permit No. 2020-0227). Mice received two intramuscular immunizations on days 0 and 14 with either the mRNA-LNP vaccine or PBS as a control. On day 33, mice were intranasally challenged with 1×10^5 PFU of the SCoV2 Omicron BA.5 variant. Two days after infection, mice were euthanized, and the lungs were collected for virological analysis. A detailed procedure is provided in the supplemental information.

Statistical analysis

Statistical analyses were performed using GraphPad Prism 8.0 (GraphPad Software Inc.). Differences between groups were considered statistically significant at $p < 0.05$.

DATA AND CODE AVAILABILITY

All data supporting the findings of this study are available within the article and its supplemental information. Additional information supporting the findings

of this study can be obtained from the corresponding author upon reasonable request.

ACKNOWLEDGMENTS

We thank the National Culture Collection for Pathogens (NCCP) at the Korean Center for Disease Control (Osong, S. Korea) for providing SCoV2 viral stocks. This study was supported by the National Research Foundation of Korea (NRF) grants (2020R1A2C2005170 and 2022M3E5F1016361) funded by the Ministry of Science and ICT (MIST), South Korea, and in part by the Ministry of Trade, Industry and Energy (MOTIE) of Korea through the Korea Institute for Advancement of Technology (KIAT) (RS-2025-23963461). H.C. was partially supported by a postdoctoral fellowship from the Brain Korea 21 (BK21) FOUR program.

AUTHOR CONTRIBUTIONS

H.Y.S. and J.-W.O. conceived and designed the experiments. H.Y.S., H.J., S.-Y.L., H.-G.J., H.C., Y.-M.S., Y.B., and S.-Y.H. conducted the experiments. H.Y.S., Y.-M.S., S.-Y.H., and H.-G.J. prepared the mRNA-LNP vaccines. H.Y.S., H.J., Y.B., and H.-G.J. performed experiments in the BSL-3 facility. H.Y.S., J.-H.K., and J.-W.O. analyzed the data. I.H.P. and J.-S.S. supervised the experiments conducted in the BSL-3 facility. H.Y.S. and J.-W.O. wrote the paper with input from the other authors. J.-W.O. supervised the studies.

DECLARATION OF INTERESTS

J.-W.O. and H.Y.S. are the inventors of the relevant patents on the mRNA vaccine candidates used in this study, which were originally filed by the University Industry Foundation (UIF) of Yonsei University, with intellectual property rights transferred to RpexBio Inc., Seoul, Korea. J.-W.O. is the founder and CEO of RpexBio Inc.

SUPPLEMENTAL INFORMATION

Supplemental information can be found online at https://doi.org/10.1016/j.omtn.2026.102886.

REFERENCES

1. Pardi, N., and Krammer, F. (2024). mRNA vaccines for infectious diseases - advances, challenges and opportunities. Nat. Rev. Drug Discov. *23*, 838–861. https://doi.org/10.1038/s41573-024-01042-y.
2. Jackson, R.J., Hellen, C.U.T., and Pestova, T.V. (2010). The mechanism of eukaryotic translation initiation and principles of its regulation. Nat. Rev. Mol. Cell Biol. *11*, 113–127. https://doi.org/10.1038/nrm2838.
3. Sample, P.J., Wang, B., Reid, D.W., Presnyak, V., McFadyen, I.J., Morris, D.R., and Seelig, G. (2019). Human 5' UTR design and variant effect prediction from a massively parallel translation assay. Nat. Biotechnol. *37*, 803–809. https://doi.org/10.1038/s41587-019-0164-5.
4. Jaafar, Z.A., and Kieft, J.S. (2019). Viral RNA structure-based strategies to manipulate translation. Nat. Rev. Microbiol. *17*, 110–123. https://doi.org/10.1038/s41579-018-0117-x.
5. Lee, K.M., Chen, C.J., and Shih, S.R. (2017). Regulation mechanisms of viral IRES-driven translation. Trends Microbiol. *25*, 546–561. https://doi.org/10.1016/j.tim.2017.01.010.
6. Xia, X. (2021). Detailed dissection and critical evaluation of the Pfizer/BioNTech and Moderna mRNA vaccines. Vaccines (Basel) *9*, 734. https://doi.org/10.3390/vaccines9070734.
7. Gebre, M.S., Rauch, S., Roth, N., Yu, J., Chandrashekar, A., Mercado, N.B., He, X., Liu, J., McMahan, K., Martinot, A., et al. (2022). Optimization of non-coding regions for a non-modified mRNA COVID-19 vaccine. Nature *601*, 410–414. https://doi.org/10.1038/s41586-021-04231-6.
8. Cho, S.H., Raybuck, A.L., Stengel, K., Wei, M., Beck, T.C., Volanakis, E., Thomas, J.W., Hiebert, S., Haase, V.H., and Boothby, M.R. (2016). Germinal centre hypoxia and regulation of antibody qualities by a hypoxia response system. Nature *537*, 234–238. https://doi.org/10.1038/nature19334.
9. Chen, Z., Han, F., Du, Y., Shi, H., and Zhou, W. (2023). Hypoxic microenvironment in cancer: molecular mechanisms and therapeutic interventions. Signal Transduct. Target. Ther. *8*, 70. https://doi.org/10.1038/s41392-023-01332-8.
10. Gan, E.S., and Ooi, E.E. (2020). Oxygen: viral friend or foe? Virol. J. *17*, 115. https://doi.org/10.1186/s12985-020-01374-2.
11. Clemens, M.J., Bushell, M., Jeffrey, I.W., Pain, V.M., and Morley, S.J. (2000). Translation initiation factor modifications and the regulation of protein synthesis in apoptotic cells. Cell Death Differ. *7*, 603–615. https://doi.org/10.1038/sj.cdd.4400695.
12. Liang, W., Gu, M., Zhu, L., Yan, Z., Schenten, D., Herrick, S., Li, H., Samrat, S.K., Zhu, J., and Chen, Y. (2023). The main protease of SARS-CoV-2 downregulates innate immunity via a translational repression. Signal Transduct. Target. Ther. *8*, 162. https://doi.org/10.1038/s41392-023-01418-3.
13. Wing, P.A.C., Keeley, T.P., Zhuang, X., Lee, J.Y., Prange-Barczynska, M., Tsukuda, S., Morgan, S.B., Harding, A.C., Argles, I.L.A., Kurlekar, S., et al. (2021). Hypoxic and pharmacological activation of HIF inhibits SARS-CoV-2 infection of lung epithelial cells. Cell Rep. *35*, 109020. https://doi.org/10.1016/j.celrep.2021.109020.
14. Wouters, B.G., and Koritzinsky, M. (2008). Hypoxia signalling through mTOR and the unfolded protein response in cancer. Nat. Rev. Cancer *8*, 851–864. https://doi.org/10.1038/nrc2501.
15. Kim, D., Lee, J.Y., Yang, J.S., Kim, J.W., Kim, V.N., and Chang, H. (2020). The architecture of SARS-CoV-2 transcriptome. Cell *181*, 914–921.e10. https://doi.org/10.1016/j.cell.2020.04.011.
16. Seo, H.Y., Jung, H., Woo, H., Jung, H.-G., Cho, H., Bak, Y., Lee, S.-Y., Son, Y.-M., Yoon, G., Hwang, S.-Y., et al. (2023). Enhanced Omicron subvariant cross-neutralization efficacy of a monovalent SARS-CoV-2 BA.4/5 mRNA vaccine encoding a noncleaved, nonfusogenic spike antigen. Preprint at bioRxiv. https://doi.org/10.1101/2023.09.10.557088.
17. Otsuka, Y., Kedersha, N.L., and Schoenberg, D.R. (2009). Identification of a cytoplasmic complex that adds a cap onto 5′-monophosphate RNA. Mol. Cell Biol. *29*, 2155–2167. https://doi.org/10.1128/MCB.01325-08.
18. Berra, E., Roux, D., Richard, D.E., and Pouysségur, J. (2001). Hypoxia-inducible factor-1 alpha (HIF-1 alpha) escapes O(2)-driven proteasomal degradation irrespective of its subcellular localization: nucleus or cytoplasm. EMBO Rep. *2*, 615–620. https://doi.org/10.1093/embo-reports/kve130.
19. Delli Ponti, R., Vandelli, A., Broglia, L., and Tartaglia, G.G. (2025). Integrating RNA structure and protein interactions to uncover the mechanisms of viral and cellular IRES function. Preprint at bioRxiv. https://doi.org/10.1101/2025.08.29.673120.
20. Cho, H., Lee, W., Kim, G.W., Lee, S.H., Moon, J.S., Kim, M., Kim, H.S., and Oh, J.W. (2019). Regulation of La/SSB-dependent viral gene expression by pre-tRNA 3' trailer-derived tRNA fragments. Nucleic Acids Res. *47*, 9888–9901. https://doi.org/10.1093/nar/gkz732.
21. Gan, W., Dai, X., Dai, X., Xie, J., Yin, S., Zhu, J., Wang, C., Liu, Y., Guo, J., Wang, M., et al. (2020). LATS suppresses mTORC1 activity to directly coordinate Hippo and mTORC1 pathways in growth control. Nat. Cell Biol. *22*, 246–256. https://doi.org/10.1038/s41556-020-0463-6.
22. Roiuk, M., Neff, M., and Teleman, A.A. (2024). eIF4E-independent translation is largely eIF3d-dependent. Nat. Commun. *15*, 6692. https://doi.org/10.1038/s41467-024-51027-z.
23. Svitkin, Y.V., Cheng, Y.M., Chakraborty, T., Presnyak, V., John, M., and Sonenberg, N. (2017). N1-methyl-pseudouridine in mRNA enhances translation through eIF2alpha-dependent and independent mechanisms by increasing ribosome density. Nucleic Acids Res. *45*, 6023–6036. https://doi.org/10.1093/nar/gkx135.
24. Silas, D.S., Juneja, B., Kaur, K., Narayanareddy Gari, M., You, Y., Moon, Y., Chen, Y., Arora, S., Hansen, J., Muthusamy, K., et al. (2024). Development of biolayer interferometry (BLI)-based double-stranded RNA detection method with application in mRNA-based therapeutics and vaccines. Pharmaceutics *16*, 1227. https://doi.org/10.3390/pharmaceutics16091227.
25. Luo, D., Wu, Z., Wang, D., Zhang, J., Shao, F., Wang, S., Cestellos-Blanco, S., Xu, D., and Cao, Y. (2023). Lateral flow immunoassay for rapid and sensitive detection of dsRNA contaminants in *in vitro*-transcribed mRNA products. Mol. Ther. Nucleic Acids *32*, 445–453. https://doi.org/10.1016/j.omtn.2023.04.005.
26. Chen, Y., Tong, P., Whiteman, N., Sanjari Moghaddam, A., Zarghami, M., Zuiani, A., Habibi, S., Gautam, A., Keerti, Bi, C., et al. (2022). Immune recall improves antibody durability and breadth to SARS-CoV-2 variants. Sci. Immunol. *7*, eabp8328. https://doi.org/10.1126/sciimmunol.abp8328.

27. Caniels, T.G., Bontjer, I., van der Straten, K., Poniman, M., Burger, J.A., Appelman, B., Lavell, A.H.A., Oomen, M., Godeke, G.J., Valle, C., et al. (2021). Emerging SARS-CoV-2 variants of concern evade humoral immune responses from infection and vaccination. Sci. Adv. *7*, eabj5365. https://doi.org/10.1126/sciadv.abj5365.

28. Cao, Y., Wang, J., Jian, F., Xiao, T., Song, W., Yisimayi, A., Huang, W., Li, Q., Wang, P., An, R., et al. (2022). Omicron escapes the majority of existing SARS-CoV-2 neutralizing antibodies. Nature *602*, 657–663. https://doi.org/10.1038/s41586-021-04385-3.

29. Wang, Q., Guo, Y., Liu, L., Schwanz, L.T., Li, Z., Nair, M.S., Ho, J., Zhang, R.M., Iketani, S., Yu, J., et al. (2023). Antigenicity and receptor affinity of SARS-CoV-2 BA.2.86 spike. Nature *624*, 639–644. https://doi.org/10.1038/s41586-023-06750-w.

30. Pardi, N., Hogan, M.J., Porter, F.W., and Weissman, D. (2018). mRNA vaccines - a new era in vaccinology. Nat. Rev. Drug Discov. *17*, 261–279. https://doi.org/10.1038/nrd.2017.243.

31. Braunstein, S., Karpisheva, K., Pola, C., Goldberg, J., Hochman, T., Yee, H., Cangiarella, J., Arju, R., Formenti, S.C., and Schneider, R.J. (2007). A hypoxia-controlled cap-dependent to cap-independent translation switch in breast cancer. Mol. Cell *28*, 501–512. https://doi.org/10.1016/j.molcel.2007.10.019.

32. Niu, D., Wu, Y., and Lian, J. (2023). Circular RNA vaccine in disease prevention and treatment. Signal Transduct. Target. Ther. *8*, 341. https://doi.org/10.1038/s41392-023-01561-x.

33. Chen, R., Wang, S.K., Belk, J.A., Amaya, L., Li, Z., Cardenas, A., Abe, B.T., Chen, C.K., Wender, P.A., and Chang, H.Y. (2023). Engineering circular RNA for enhanced protein production. Nat. Biotechnol. *41*, 262–272. https://doi.org/10.1038/s41587-022-01393-0.

34. Hwang, H.J., and Kim, Y.K. (2024). Molecular mechanisms of circular RNA translation. Exp. Mol. Med. *56*, 1272–1280. https://doi.org/10.1038/s12276-024-01220-3.

35. Greenberger, J.S., Hou, W., Shields, D., Fisher, R., Epperly, M.W., Sarkaria, I., Wipf, P., and Wang, H. (2024). SARS-CoV-2 Spike protein induces oxidative stress and senescence in mouse and human lung. In Vivo *38*, 1546–1556. https://doi.org/10.21873/invivo.13605.

36. Panwar, V., Singh, A., Bhatt, M., Tonk, R.K., Azizov, S., Raza, A.S., Sengupta, S., Kumar, D., and Garg, M. (2023). Multifaceted role of mTOR (mammalian target of rapamycin) signaling pathway in human health and disease. Signal Transduct. Target. Ther. *8*, 375. https://doi.org/10.1038/s41392-023-01608-z.

37. Slobodin, B., Sehrawat, U., Lev, A., Hayat, D., Zuckerman, B., Fraticelli, D., Ogran, A., Ben-Shmuel, A., Bar-David, E., Levy, H., et al. (2022). Cap-independent translation and a precisely located RNA sequence enable SARS-CoV-2 to control host translation and escape anti-viral response. Nucleic Acids Res. *50*, 8080–8092. https://doi.org/10.1093/nar/gkac615.

38. Aviner, R., Lidsky, P.V., Xiao, Y., Tassetto, M., Kim, D., Zhang, L., McAlpine, P.L., Elias, J., Frydman, J., and Andino, R. (2024). SARS-CoV-2 Nsp1 cooperates with initiation factors EIF1 and 1A to selectively enhance translation of viral RNA. PLoS Pathog. *20*, e1011535. https://doi.org/10.1371/journal.ppat.1011535.

39. Malone, B., Urakova, N., Snijder, E.J., and Campbell, E.A. (2022). Structures and functions of coronavirus replication-transcription complexes and their relevance for SARS-CoV-2 drug design. Nat. Rev. Mol. Cell Biol. *23*, 21–39. https://doi.org/10.1038/s41580-021-00432-z.

40. Yueh, A., and Schneider, R.J. (2000). Translation by ribosome shunting on adenovirus and hsp70 mRNAs facilitated by complementarity to 18S rRNA. Genes Dev. *14*, 414–421.

41. Flynn, R.A., Belk, J.A., Qi, Y., Yasumoto, Y., Wei, J., Alfajaro, M.M., Shi, Q., Mumbach, M.R., Limaye, A., DeWeirdt, P.C., et al. (2021). Discovery and functional interrogation of SARS-CoV-2 RNA-host protein interactions. Cell *184*, 2394–2411.e16. https://doi.org/10.1016/j.cell.2021.03.012.

42. Mulroney, T.E., Pöyry, T., Yam-Puc, J.C., Rust, M., Harvey, R.F., Kalmar, L., Horner, E., Booth, L., Ferreira, A.P., Stoneley, M., et al. (2024). N(1)-methylpseudouridylation of mRNA causes +1 ribosomal frameshifting. Nature *625*, 189–194. https://doi.org/10.1038/s41586-023-06800-3.

43. Monroe, J., Eyler, D.E., Mitchell, L., Deb, I., Bojanowski, A., Srinivas, P., Dunham, C.M., Roy, B., Frank, A.T., and Koutmou, K.S. (2024). N1-Methylpseudouridine and pseudouridine modifications modulate mRNA decoding during translation. Nat. Commun. *15*, 8119. https://doi.org/10.1038/s41467-024-51301-0.

44. Tang, J., Zeng, C., Cox, T.M., Li, C., Son, Y.M., Cheon, I.S., Wu, Y., Behl, S., Taylor, J.J., Chakaraborty, R., et al. (2022). Respiratory mucosal immunity against SARS-CoV-2 after mRNA vaccination. Sci. Immunol. *7*, eadd4853. https://doi.org/10.1126/sciimmunol.add4853.

45. Israelow, B., Mao, T., Klein, J., Song, E., Menasche, B., Omer, S.B., and Iwasaki, A. (2021). Adaptive immune determinants of viral clearance and protection in mouse models of SARS-CoV-2. Sci. Immunol. *6*, eabl4509. https://doi.org/10.1126/sciimmunol.abl4509.

46. Zhang, Y., Wu, Y., Zhang, M.Q., Rao, H., Zhang, Z., He, X., Liang, Y., Guo, R., Yuan, Y., Sun, J., et al. (2025). An RBD-Fc mucosal vaccine provides variant-proof protection against SARS-CoV-2 in mice and hamsters. npj Vaccines *10*, 100. https://doi.org/10.1038/s41541-025-01155-4.

47. Casadevall, A., and Focosi, D. (2025). Lessons from the use of monoclonal antibodies to SARS-CoV-2 Spike protein during the COVID-19 pandemic. Annu. Rev. Med. *76*, 1–12. https://doi.org/10.1146/annurev-med-061323-073837.

48. Kim, M., Lee, Y.J., Yoon, J.S., Ahn, J.Y., Kim, J.H., Choi, J.Y., and Oh, J.W. (2021). Genome sequences of two GH clade SARS-CoV-2 strains isolated from patients with COVID-19 in South Korea. Microbiol. Resour. Announc. *10*, e01384-20. https://doi.org/10.1128/MRA.01384-20.

49. Lee, W., Lee, S.H., Kim, M., Moon, J.S., Kim, G.W., Jung, H.G., Kim, I.H., Oh, J.E., Jung, H.E., Lee, H.K., et al. (2018). Vibrio vulnificus quorum-sensing molecule cyclo(Phe-Pro) inhibits RIG-I-mediated antiviral innate immunity. Nat. Commun. *9*, 1606. https://doi.org/10.1038/s41467-018-04075-1.

50. Pisal, R.V., Hrebíková, H., Chvátalová, J., Kunke, D., Filip, S., and Mokrý, J. (2016). Detection of mycoplasma contamination directly from culture supernatant using polymerase chain reaction. Folia Biol. *62*, 203–206. https://doi.org/10.14712/fb2016062050203.

51. Kim, M., Cho, H., Ahn, D.G., Jung, H.G., Seo, H.Y., Kim, J.S., Lee, Y.J., Choi, J.Y., Park, I.H., Shin, J.S., et al. (2021). In vitro replication inhibitory activity of xanthorrhizol against severe acute respiratory syndrome coronavirus 2. Biomedicines *9*, 1725. https://doi.org/10.3390/biomedicines9111725.

52. Ball, R.L., Bajaj, P., and Whitehead, K.A. (2017). Achieving long-term stability of lipid nanoparticles: examining the effect of pH, temperature, and lyophilization. Int. J. Nanomedicine *12*, 305–315. https://doi.org/10.2147/IJN.S123062.

53. Muramatsu, H., Lam, K., Bajusz, C., Laczkó, D., Karikó, K., Schreiner, P., Martin, A., Lutwyche, P., Heyes, J., and Pardi, N. (2022). Lyophilization provides long-term stability for a lipid nanoparticle-formulated, nucleoside-modified mRNA vaccine. Mol. Ther. *30*, 1941–1951. https://doi.org/10.1016/j.ymthe.2022.02.001.